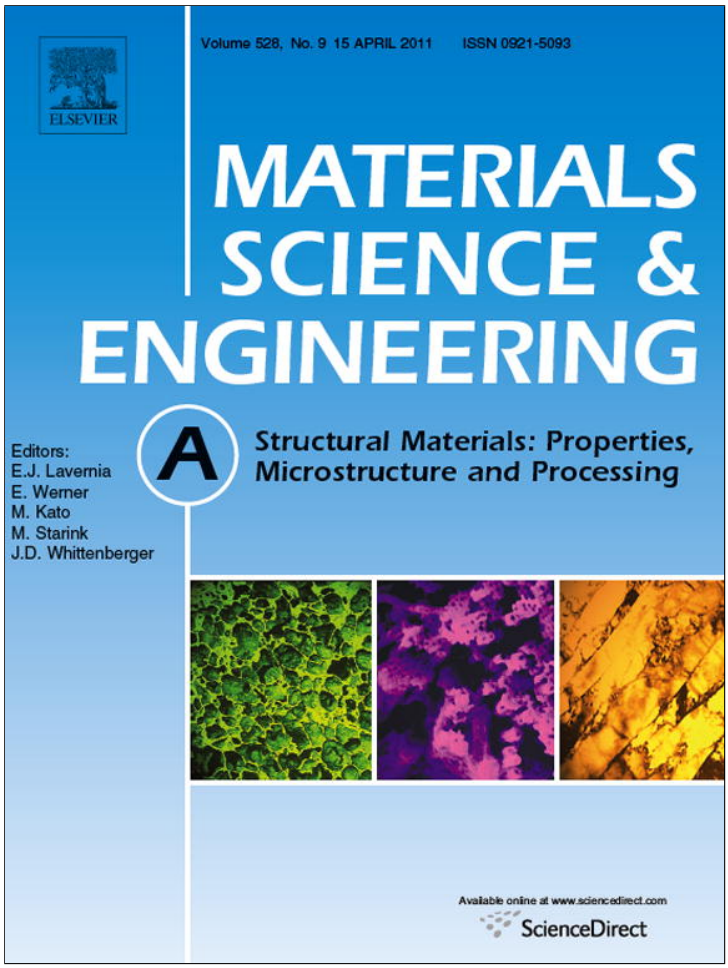

Materials Science and Engineering A 528 (2011) 3513–3519

Contents lists available at ScienceDirect

Materials Science and Engineering A

journal homepage: www.elsevier.com/locate/msea

Composition and orientation effects on the final recrystallization texture of coarse-grained Nb-containing AISI 430 ferritic stainless steels

R.P. Siqueira [a], H.R.Z. Sandim [a,*], T.R. Oliveira [b], D. Raabe [c]

[a] Departamento de Engenharia de Materiais, Escola de Engenharia de Lorena, University of Sao Paulo, 12600-970, Lorena-SP, Brazil
[b] Centro de Pesquisa da ArcelorMittal Inox Brasil S.A., 35180-000, Timóteo-MG, Brazil
[c] Max-Planck Institut für Eisenforschung, D-40237, Düsseldorf, Germany

ARTICLE INFO

Article history:
Received 17 December 2010
Accepted 5 January 2011
Available online 12 January 2011

Keywords:
Hot-band
Texture
Recrystallization
Composition effects
Coarse grain
Ferritic stainless steel

ABSTRACT

Composition and orientation effects on the final recrystallization texture of three coarse-grained Nb-containing AISI 430 ferritic stainless steels (FSSs) were investigated. Hot-bands of steels containing distinct amounts of niobium, carbon and nitrogen were annealed at 1250 °C for 2 h to promote grain growth. In particular, the amounts of Nb in solid solution vary from one grade to another. For purposes of comparison, the texture evolution of a hot-band sheet annealed at 1030 °C for 1 min (finer grain structure) was also investigated. Subsequently, the four sheets were cold rolled up to 80% reduction and then annealed at 800 °C for 15 min. Texture was determined using X-ray diffraction and electron backscatter diffraction (EBSD). Noticeable differences regarding the final recrystallization texture and microstructure were observed in the four investigated grades. Results suggest that distinct nucleation mechanisms take place within these large grains leading to the development of different final recrystallization textures.

1. Introduction

Ferritic stainless steels (FSSs) have good corrosion resistance, particularly to chloride stress corrosion cracking, and appropriate formability during deep drawing [1–4]. In this paper, the texture evolution of AISI 430 FSSs containing 16% chromium and different amounts of niobium, carbon and nitrogen was investigated. Niobium improves mechanical properties such as creep and thermal fatigue resistances and it also avoids sensitization in the heat-affected zone of welded parts. Niobium plays two important roles in the microstructure of ferritic stainless steels. Niobium reacts with interstitials dissolved in the ferrite matrix leaving the steel free from interstitial C and N atoms. Precipitates such as Nb(C,N), Fe_2Nb and Fe_3Nb_3C were reported in Nb-containing FSSs depending on their composition [5,6]. Recent papers have also demonstrated that solid solution niobium, even in small amounts, is very effective to slow boundary migration during recrystallization and grain growth [7,8].

Alloyed ferritic steels (e.g. Fe–16 wt.% Cr and Fe–3 wt.% Si) and low-carbon ferritic steels reveal similarities in terms of the recrystallization texture evolution [9–13]. During typical industrial steel processing, bcc (body-centered cubic) steels are after initial hot rolling cold rolled up to approximately 80% thickness reduction and annealed subsequently to achieve primary static recrystallization [9–14]. The cold rolling textures of bcc steels can be described by a set of texture fibers such as the α-fiber collecting all grains with a ⟨1 1 0⟩ direction parallel to the rolling direction and the γ-fiber summarizing all crystals with a {1 1 1} plane parallel to the sheet surface [9–15]. The α-fiber texture strengthens during cold rolling leading to pronounced maxima at the {0 0 1}⟨1 1 0⟩, {1 1 2}⟨1 1 0⟩, and {1 1 1}⟨1 1 0⟩ texture components at strains of about 80% sheet thickness reduction [14]. After subsequent primary static recrystallization annealing, the orientation density of the α-fiber decays between {0 0 1}⟨1 1 0⟩ and {1 1 2}⟨1 1 0⟩ and the intensity of the γ-fiber texture increases leading to maxima around the {1 1 1}⟨1 1 2⟩ and {1 1 1}⟨1 1 0⟩ components (at sufficiently high preceding strains above 50%). Hence, in general {1 1 1}⟨*u v w*⟩ components characterize typical recrystallization textures observed in bcc metals [9–14]. A high and equally distributed intensity of the {1 1 1}⟨*u v w*⟩ texture and a topologically random arrangement of the γ-fiber crystallites is usually pursued to enhance formability under stretching and drawing constraints [4].

The literature shows that the hot rolling in the ferritic region can enhance the deep drawability [16]. For high-alloyed steels such as FSSs, the formability is slightly lower than the one observed for low carbon steel sheets [17–20]. It was found that both, hot-band annealing or intermediate annealing during cold rolling can increase the γ-fiber texture after recrystallization annealing improving the overall forming properties under stretching and drawing loading conditions. In addition, previous studies suggest

* Corresponding author. Tel.: +55 12 3159 9916; fax: +55 12 3153 3006.
E-mail address: hsandim@demar.eel.usp.br (H.R.Z. Sandim).

0921-5093/$ – see front matter © 2011 Elsevier B.V. All rights reserved.
doi:10.1016/j.msea.2011.01.007

Table 1
Chemical composition of the Nb-containing ferritic stainless steels (in wt.%).

Steel type	Cr	Nb	C	N	Mn	Si	P
FSS-A	16.14	0.31	0.02	0.02	0.16	0.29	0.03
FSS-B	16.22	0.37	0.02	0.02	0.15	0.30	0.03
FSS-C	16.23	0.56	0.03	0.03	0.15	0.24	0.03
FSS-R	16.29	0.38	0.02	0.02	0.19	0.34	0.03

that the ridging phenomenon is minimized which is beneficial for further drawing operations, particularly for surface appearance and the forming limits [21–23]. Ridging which is sometimes also referred to as roping is a microstructural effect which manifests itself in the formation of a corrugated surface profile that maps the longitudinal alignment of grain clusters of different mechanical properties [12,24]. In bcc steels these are usually large $\{0\,0\,1\}\langle 1\,1\,0\rangle$ oriented grain clusters that are inherited form the hot band microstructure and in fcc (face-centered cubic) metals such as 6xxx Al alloys these are usually elongated near-$\{0\,0\,1\}\langle 1\,0\,0\rangle$-oriented grain clusters [24].

For grain-oriented silicon steels, after recrystallization, further high-temperature annealing is carried out in order to promote the formation of a sharp $\{0\,1\,1\}\langle 0\,0\,1\rangle$ Goss texture component through secondary recrystallization [25]. In this case, hot-band annealing can influence both the resulting primary and secondary recrystallization texture. The results show that the Goss texture increases after secondary recrystallization annealing [26].

In this paper, we investigate both composition and orientation effects in the final recrystallization annealing texture of three Nb-containing AISI 430 FSSs. Grades A, B, and C differ from each other with regard to the initial texture and to the amounts of Nb in solid solution (0.03, 0.09 and 0.14 wt.%, respectively). The final recrystallization texture and the microstructure vary significantly from one grade to another due to the coarse-grained microstructure obtained after hot-band annealing at 1250 °C for 2 h.

2. Experimental

The 4-mm thick Nb-containing FSS hot bands were supplied by ArcelorMittal Inox Brasil S.A. Hot bands of grades referred to as FSS-A, FSS-B, and FSS-C were annealed at 1250 °C for 2 h (high-temperature annealing) to obtain coarse-grained materials. The three steel grades differ mostly in the Nb and interstitial contents (0.31–0.56 wt.%. Nb), namely, steel FSS-A has 0.31 wt.% Nb, steel FSS-B has 0.37 wt.% Nb, and steel FSS-C has 0.56 wt.% Nb. The full chemical composition of these steels is shown in Table 1. For purposes of comparison, we have also investigated the annealing behavior of a hot band of a reference steel (FSS-R) annealed at 1030 °C for 1 min to promote static recrystallization. This reference steel was processed following industrial parameters. Two other important parameters to compare the different grades used in the present investigation are the ratio Nb/(C + N) and the amount of Nb in solid solution (Nb_{ss}). The latter is calculated using the simple expression $Nb_{ss} = Nb_t - 7(C + N)$, where Nb_t is the total amount of niobium and C + N the sum of the amounts of carbon and nitrogen, given in wt.% [1]. These parameters are displayed in Table 2. After hot rolling and hot band annealing all annealed hot bands, including FSS-R, were cold rolled up to 80% thickness reduction ($\varepsilon \approx 1.6$) and annealed at 800 °C for 15 min to promote final recrystallization. Grain size was determined using the linear intercept method. Fig. 1 summarizes the experimental procedure used in this work.

Table 2
Nb/(C + N) ratios and respective amounts of niobium in solid solution found in grades FSS-A, FSS-B, FSS-C and FSS-R.

Grade	C + N (wt.%)	Nb/(C + N)	Nb_{ss} (wt.%)
FSS-A	0.04	7.75	0.03
FSS-B	0.04	9.25	0.09
FSS-C	0.06	9.33	0.14
FSS-R	0.04	9.5	0.10

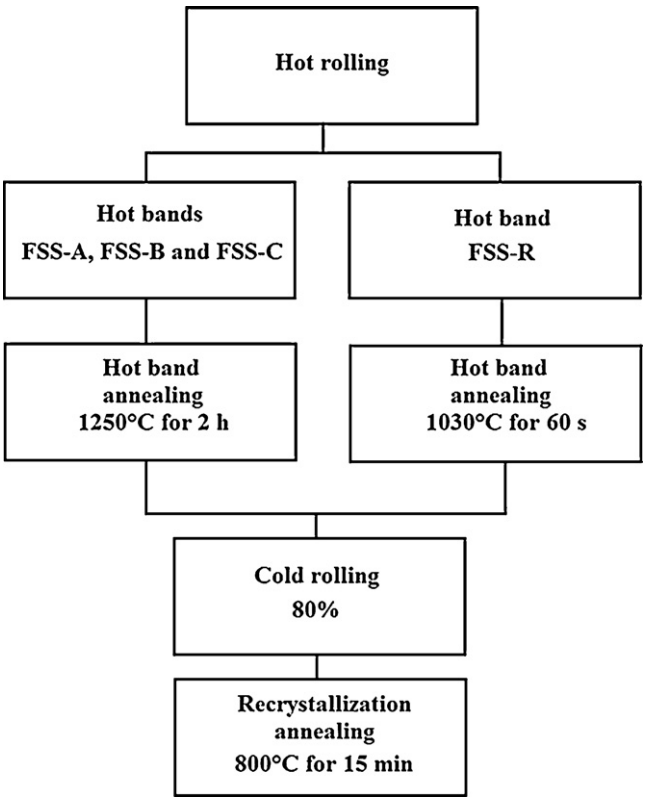

Fig. 1. Block diagram showing the thermomechanical processing used in this work. Ferritic stainless steels referred to FSS-A, B and C have coarse-grained structures. FSS-R has a finer grain structure.

Microstructural characterization was carried out in the rolling plane using a LEO 1450-VP SEM operated at 20 kV in the backscattered electrons mode (BSE). The EBSD scans were performed in a Philips XL-30 SEM operated at 20 kV with a LaB_6 filament. Microtexture data were evaluated using the EDAX-TSL software package. A map step size of 1 μm was used. The black and white lines mark high-angle (>15° misorientation) and low-angle boundaries (<15° misorientation), respectively, in all scans. The orientation distribution function (ODF) and pole figures (PF) were determined by the discrete-binning method from the EBSD data. The texture was evaluated by conventional X-ray texture analysis using a Philips X'Pert PRO MPD texture diffractometer with a Cu Kα radiation. The ODFs ($\varphi_2 = 0°$ and 45°) were calculated from three pole figures (2 0 0), (1 1 0), and (2 1 1) using the FHM software system [27]. The orientations are expressed in the Euler angles using the Bunge

Table 3
Main texture components for ferritic stainless steels after thermomechanical processing.

Miller indices $\{h\,k\,l\}\langle u\,v\,w\rangle$	Name	Symbol	Bunge notation $(\Phi, \varphi_1, \varphi_2)$
$\{0\,0\,1\}\langle 0\,1\,1\rangle$	45°-rotated cube	H	(0°,45°,0°) or (0°,0°,45°)
$\{0\,0\,1\}\langle 0\,2\,1\rangle$	–	CH	(0°,26°,0°)
$\{0\,1\,1\}\langle 0\,0\,1\rangle$	Goss	G	(45°,0°,0°) or (90°,90°,45°)
$\{0\,1\,1\}\langle 2\,1\,1\rangle$	Brass	B	(45°,35°,0°)
$\{0\,2\,1\}\langle 0\,0\,1\rangle$	–	CG	(26°,0°,0°)
$\{4\,4\,11\}\langle 11\,11\,8\rangle$	Taylor	T	(27°,90°,45°)

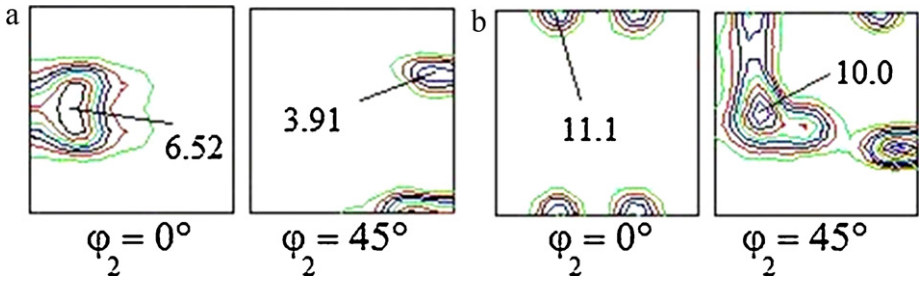

Fig. 2. ODFs showing the texture of the fine-grained reference steel (FSS-R) after hot-rolling and hot-band annealing at 1030 °C for 60 s: (a) surface layer and (b) center layer.

notation (φ_1, Φ, φ_2). EBSD was performed in longitudinal sections in all scans after metallographic preparation. Table 3 displays the main texture components observed in all specimens after thermo-mechanical processing. In order to investigate the texture changes through the thickness, texture measurements were carried out at both center and surface layers [9].

3. Results and discussion

3.1. Microstructure of the annealed hot bands

A detailed description of both microstructure and texture of FSS-A, FSS-B and FSS-C sheets after hot-band annealing at 1250 °C for 2 h is shown elsewhere [28]. The average grain sizes for FSS-A and FSS-B are, respectively, 1200 ± 200 and 1000 ± 200 μm. The average grain size for FSS-C is 650 ± 80 μm. FSS-A and FSS-B have quite similar chemical compositions (0.31 and 0.37 wt.% Nb, respectively) whereas FFS-C contains much more Nb (0.56 wt.%) and interstitials (carbon and nitrogen). These results show that increasing amounts of niobium, carbon and nitrogen lead to grain refinement. At 1250 °C, most of the particles (Nb C,N) are expected to be dissolved [29] indicating that solute drag rather than Zener drag is responsible for the observed differences in grain size. In contrast, the grain structure of the hot band reference steel annealed at 1030 °C for 1 min is rather uniform and much finer (23 ± 5 μm). The chemical composition of this grade is similar to FSS-B. In this case, the finer grain size can be attributed to the lower hot-band annealing temperature.

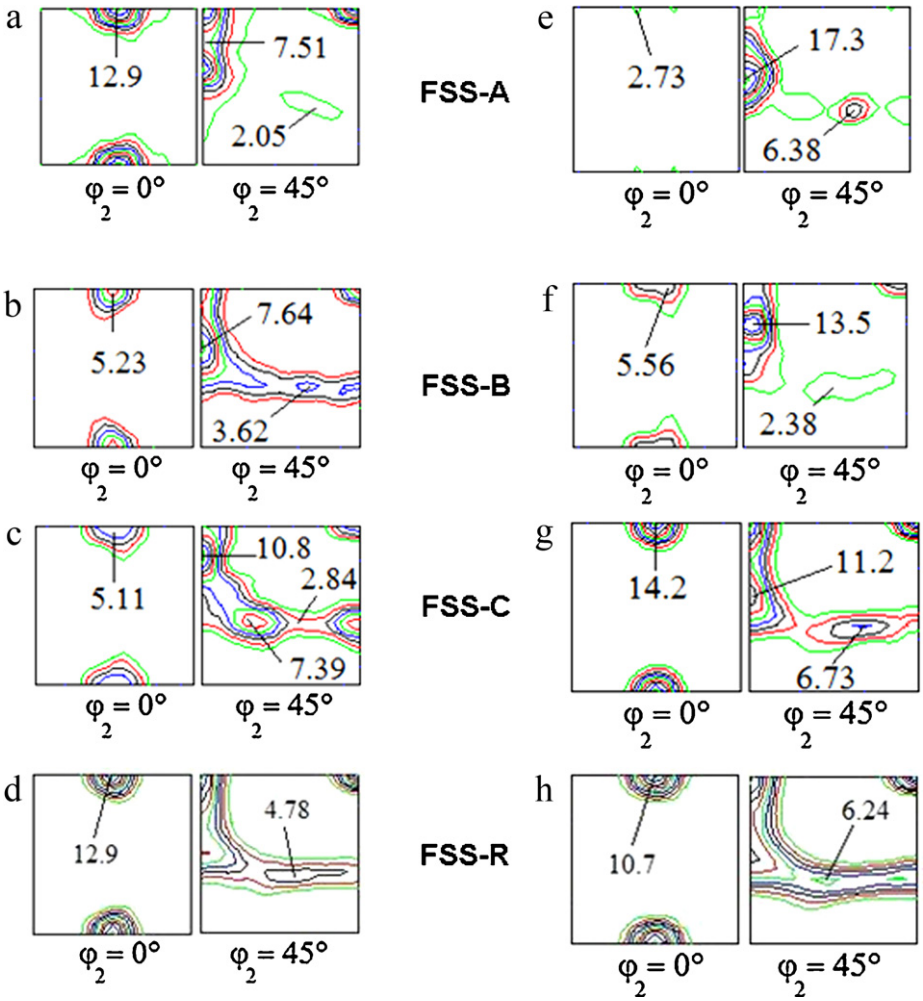

Fig. 3. ODFs showing the texture of 80% cold-rolled Nb-containing ferritic stainless steels (FSSs): (a–d) surface layer, (e–h) center layer. Ferritic stainless steels referred to FSS-A, B and C have coarse-grained structures. FSS-R has a finer grain structure.

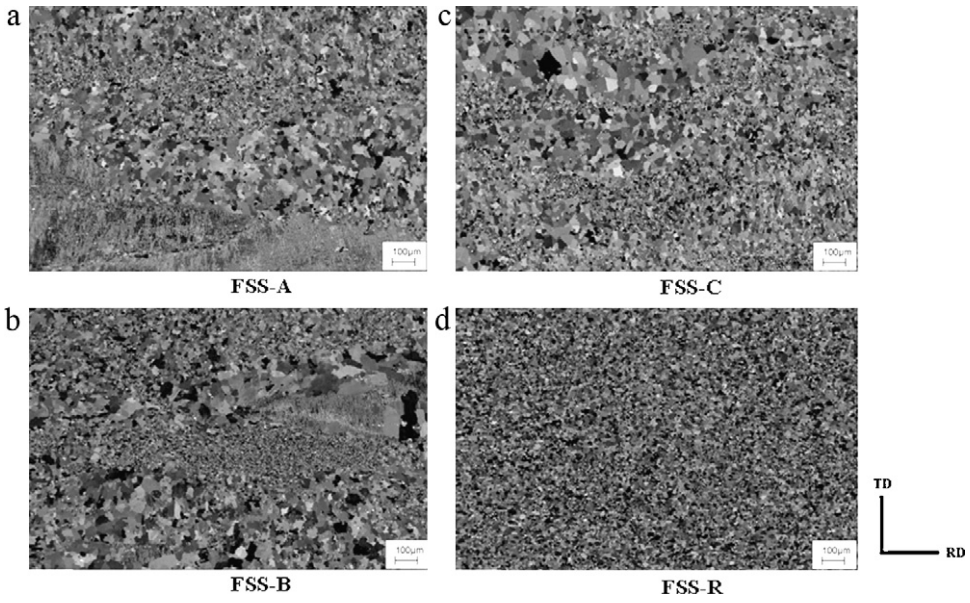

Fig. 4. SEM micrographs (backscattered electrons) showing the microstructure of Nb-containing ferritic stainless steels (FSSs) after final recrystallization annealing: coarse-grained (a) FSS-A; (b) FSS-B; (c) FSS-C; and fine-grained (d) FSS-R.

3.2. Texture of the annealed hot bands (reference steel)

Fig. 2 shows the texture evolution of the reference steel after hot-rolling and further annealing at 1030 °C for 1 min. This annealed sheet shows strong texture components that vary from the surface to the center layers. In the surface layer (Fig. 2a), the main texture components belong to the $\{0\,1\,1\}\langle u\,v\,v\rangle$ (Goss-to-Brass) fiber axis and to the $\{4\,4\,11\}\langle 11\,11\,8\rangle$ bcc shear texture Taylor component. These orientations are known as main shear-deformation induced texture components in bcc metals [9,30,31]. Typically such heavily sheared surface and sub-surface bcc texture components are also prone to undergo (partial) recrystallization during hot rolling owing to the larger amount of deformation that is usually accumulated within the surface and sub-surface layers [9–13,30,31]. In the center layer (Fig. 2b), the main texture components observed are $\{0\,0\,1\}\langle 1\,2\,0\rangle$ (CH) and γ-fiber components. These texture components were also observed in hot bands of grades FSS-A, FSS-B and FSS-C annealed at 1250 °C for 2 h [28].

3.3. Cold rolling texture

The annealed hot-bands were cold rolled up to 80% thickness reduction. During cold rolling, strong α- and γ-fiber textures develop for all compositions investigated in both surface and cen-

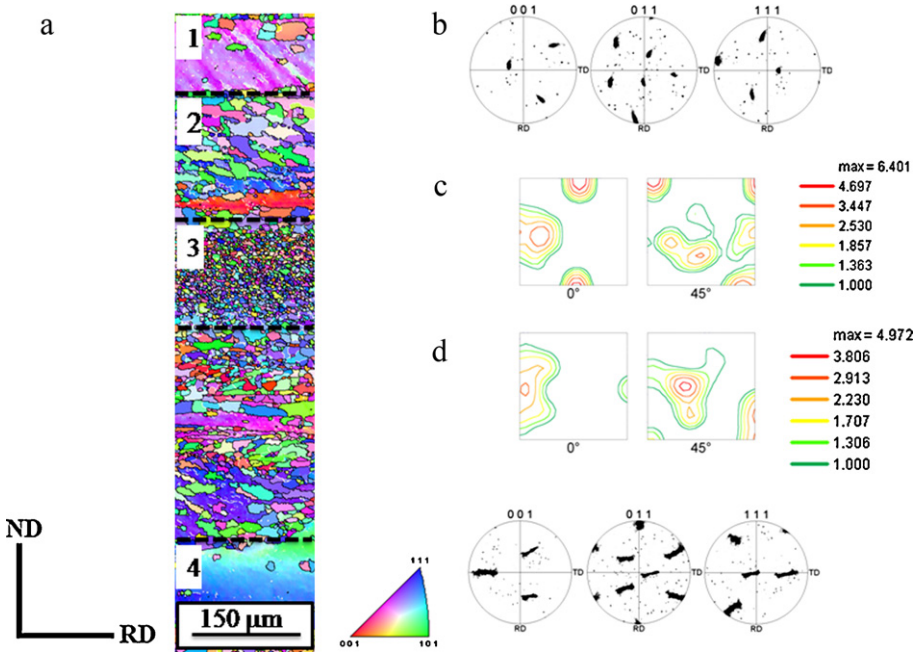

Fig. 5. EBSD results showing the inhomogeneous recrystallization behavior in FSS-A after final recrystallization annealing: (a) orientation map; (b) pole figures corresponding to partial-recrystallized region 1; (c and d) ODFs (φ_2-constant sections) corresponding to distinct recrystallized regions 2 and 3, respectively and (e) pole figures corresponding to recovered region 4.

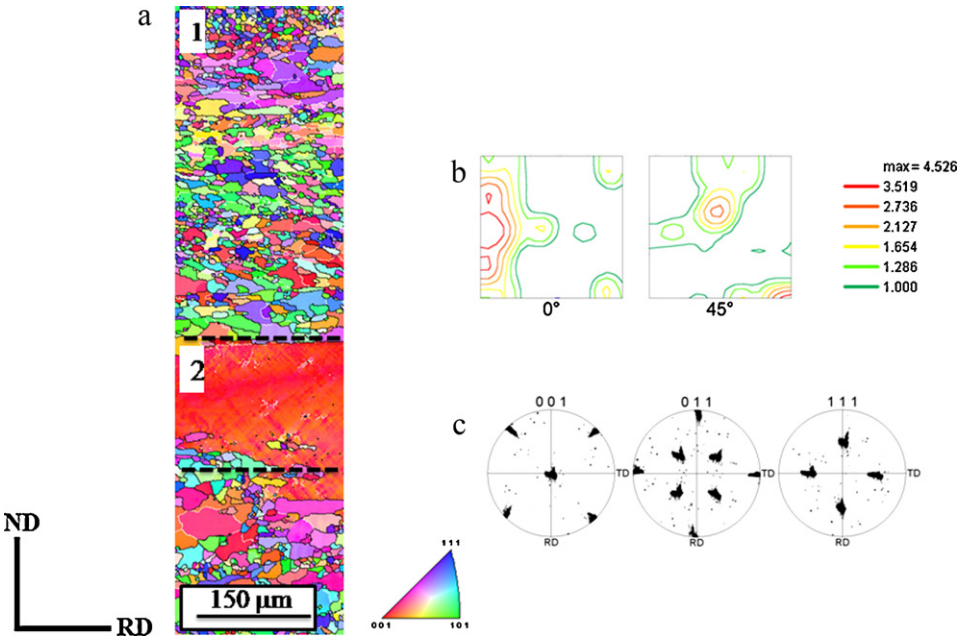

Fig. 6. EBSD results showing the inhomogeneous recrystallization behavior in FSS-B after final recrystallization annealing: (a) orientation map; (b) ODF (φ_2-constant sections) corresponding to recrystallized region 1 and (c) pole figures corresponding to recovered region 2.

ter layers [9,30,31]. The main texture components of grades FSS-A and FSS-B after 80% cold rolling are $\{1\,0\,0\}\langle 0\,1\,1\rangle$ (rotated cube) and $\{1\,1\,2\}\langle 0\,1\,1\rangle$ in the surface layer (Fig. 3a and b). For the FSS-A, the γ-fiber texture after 80% cold rolling is not complete, whereas for the steel FSS-B the γ-fiber texture is complete showing a homogeneous orientation density along the $\langle 1\,1\,1\rangle$ fiber after 80% thickness reduction. For FSS-C (Fig. 3c), a strong $\{1\,1\,1\}\langle 1\,1\,2\rangle$ and a 45° rotated cube texture component are present. Texture components close to the ideal $\{0\,1\,1\}\langle u\,v\,v\rangle$ fiber are very unstable under plane strain loads [32] and tend to rotate about the $\langle 1\,1\,0\rangle$ axis into either the 45° rotated cube component or the $\{1\,1\,1\}\langle 1\,1\,2\rangle$ orientation [30]. In the center layer (Fig. 3e–g), the α-fiber texture is stronger than at the surface layer. We have also observed that the 45° rotated cube component becomes stronger for higher contents of Nb, C and N, whereas CH components disappear during cold rolling. Tsuji et al. have reported similar results in cold-rolled Nb-free 19% Cr FSS [33]. They showed that $(0\,0\,1)[5\,1\,0]$–$(0\,0\,1)[3\,2\,0]$ oriented grains rotated towards the $(001)[1\,1\,0]$ α-fiber component, whereas $(0\,0\,1)[1\,1\,0]$ and $(0\,0\,1)[1\,0\,0]$ tend to keep their initial orientations after cold rolling. The γ-fiber texture components are also present at the center layer, however, these components remain quite weak. Only orientations close to $\{1\,1\,1\}\langle 0\,1\,1\rangle$ belong-

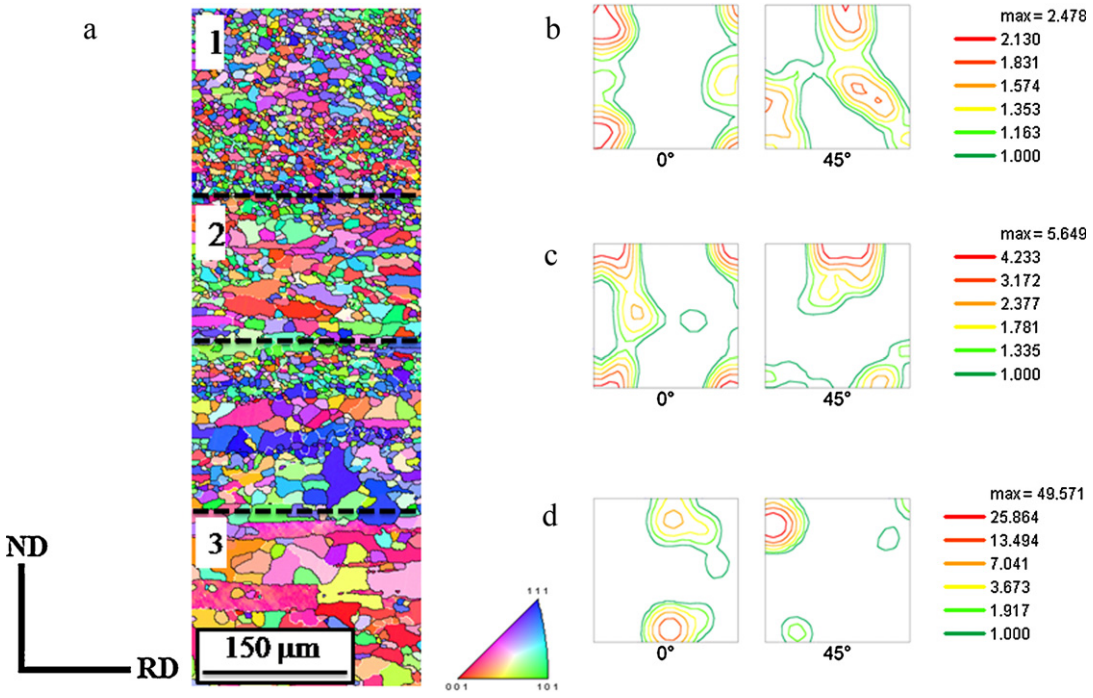

Fig. 7. EBSD results showing inhomogeneous recrystallization behavior in FSS-C after final recrystallization annealing: (a) orientation map; (b–d) ODF (φ_2-constant sections) corresponding to distinct recrystallized regions 1, 2, and 3, respectively.

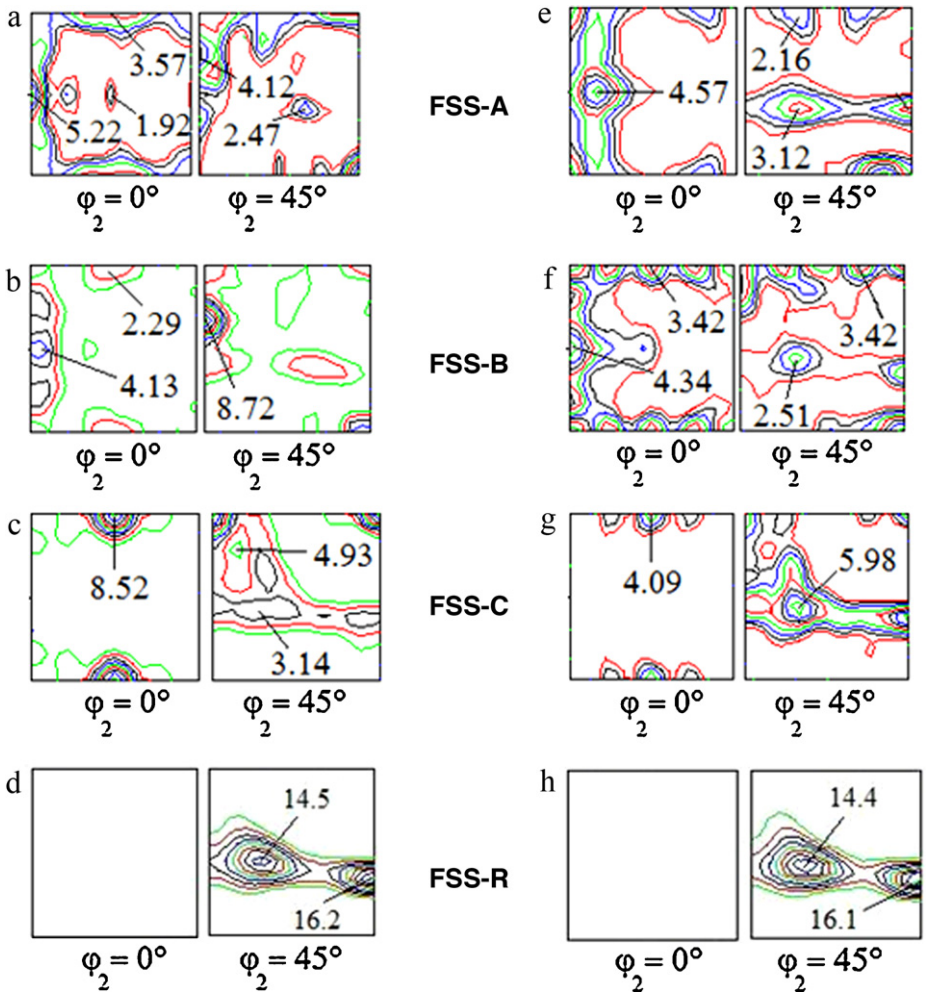

Fig. 8. ODFs showing the texture of 80% cold-rolled Nb-containing ferritic stainless steels after final recrystallization annealing at 800 °C for 15 min: (a–d) surface layer, (e–h) center layer. Ferritic stainless steels referred to FSS-A, B and C have coarse-grained structures. FSS-R has a finer grain structure.

ing to both the α- and γ-fibers show high intensity. The reference steel (Fig. 3d and h) shows both a sharp α-fiber with high orientation density close to both the 45° rotated cube component and the {1 1 1}⟨1 1 0⟩ texture component as well as a complete γ-fiber.

3.4. Microstructure after final recrystallization annealing

The 80% cold-rolled sheets of the four investigated grades were annealed at 800 °C for 15 min to promote final recrystallization. Fig. 4 shows the resulting microstructures. Regarding FSS-A, FSS-B and FSS-C grades (Fig. 4a–c), the recrystallization behavior varies among these steels. Due to orientation effects enhanced by the starting coarse-grained structure inherited form the respective hot bands, important differences in terms of final recrystallized grain size and recrystallized volume fraction were observed. For FSS-A, the least alloyed grade, an inhomogeneous microstructure is found. It consists of regions where recrystallized and recovered areas are found in close vicinity. It is worth mentioning that the grain size also varies significantly from one recrystallized region to another. The width of these areas is equivalent to the grain size of the 80% cold-rolled sheets, i.e. they reflect the behavior of individual grains in the annealed hot-band (Fig. 4a) [9]. For FSS-B (Fig. 4b), the microstructure shows a lower fraction of recovered areas, whereas in FSS-C (Fig. 4c) the microstructure is fully recrystallized but with a non-uniform grain size distribution.

Orientation effects in the recrystallization behavior of bcc metals were often reported in the literature [34–36]. These effects can be studied particularly in samples with coarse grains. Large crystals make important differences visible in terms of the developed substructure and stored energy as a function of their orientation. Nucleation of recrystallization is strongly dependent on the nature of the grain subdivision mechanisms acting within a grain. Deformation banding, for instance, is known to be orientation and grain-size dependent [37] and provides a large number of mobile high-angle boundaries to trigger recrystallization in coarse-grained metals [38]. In the present work, EBSD was used to demonstrate these orientation effects in grades FSS-A to FSS-C. A close observation in the orientation image maps of these samples reveals the presence of recovered and recrystallized areas coexisting in the annealed microstructure. Grain size and texture vary locally as a direct effect of the initial orientation of each grain. Representative examples of such non-uniform microstructures are shown in Figs. 5–7. Fig. 5 shows a longitudinal section of the FSS-A sheet after 80% cold rolling and further recrystallization annealing at 800 °C for 15 min. Four regions were chosen to demonstrate orientation effects. Region 1 shows a banded substructure and partial recrystallization. The orientation of the recovered matrix is also shown. Regions 2 and 3 are adjacent to each other and reveal a fully recrystallized microstructure. They differ, however, in terms of the grain size and the microtexture. Region 4 is also partially recrystallized. These microstructure observations confirm the presence of pro-

nounced orientation effects. Fig. 6 refers to FSS-B and shows two regions with distinct annealing behaviors. In the recrystallized part of the sample (region 1), Goss and CH components are present. The recovered grain (region B) corresponds to a 45° rotated cube grain [39]. A few grains within the dashed square were nucleated by particle stimulated nucleation (PSN) around coarse Nb(C,N) particles. Similar features regarding grain-to-grain texture gradients are found in fully recrystallized FSS-C (Fig. 7). Notice that texture significantly varies locally in terms of the components and corresponding intensities.

In contrast, the microstructure of the reference steel is much more uniform with a recrystallized grain size of 9 ± 1 μm (Fig. 4d). Orientation effects in this case are much less pronounced due to a much more uniform distribution of stored energy after cold rolling.

3.5. Recrystallization texture

3.5.1. Surface layer

The final recrystallization textures of the grades FSS-A, FSS-B and FSS-C (Fig. 8) annealed at 800 °C for 15 min show distinct texture components. In the surface layer (Fig. 8a–c), the orientations spread around some ideal components such as Goss orientation, the $\{0\,0\,1\}\langle u\,v\,0\rangle$ fiber (referred to as η-fiber), and the 45° rotated cube. The spreads around the 45° rotated cube and Goss components tend to decrease as the contents of Nb, C and N increase. In FSS-C, for instance, the Goss component is absent. These components are undesirable for further drawing operations [15]. For the high-alloyed grade (FSS-C), the texture remains unchanged during annealing and displays α- and γ-fiber texture components, however, new components close to $\{1\,1\,2\}\langle 1\,3\,1\rangle$ become noticeable. It can be also observed that the 45° rotated-cube texture component is pronounced (about 9 times random).

3.5.2. Center layer

In the center layer (Fig. 8e–g), the α-fiber texture components tend to disappear for decreasing Nb and interstitial contents, whereas the γ-fiber texture components become stronger with a maximum at $\{1\,1\,1\}\langle 1\,1\,2\rangle$ with increasing Nb and interstitial contents. The CH-$\{0\,0\,1\}\langle 1\,2\,0\rangle$-texture component appears after final recrystallization annealing for grades A, B and C in the center layer. Similar results can be observed to Fe3%Si after recrystallization annealing [9,10,40]. The results suggest that, during recrystallization annealing of the cold-rolled coarse grains, new recrystallization nuclei belonging to the $\{0\,0\,1\}\langle 1\,2\,0\rangle$-texture component seems arise from the remaining coarse fragmented CH-oriented grains.

3.5.3. Reference steel (FSS-R)

The texture observed in the reference steel (Fig. 8d and h) after final recrystallization annealing shows that the α-fiber components between $\{0\,0\,1\}\langle 1\,1\,0\rangle$ and $\{1\,1\,2\}\langle 1\,1\,0\rangle$ disappear and the intensity of the γ-fiber texture increases leading to a maximum around $\{1\,1\,1\}\langle 1\,1\,2\rangle$ [10]. This component ($\{1\,1\,1\}\langle u\,v\,w\rangle$) is very suitable for deep-drawing operations. Raabe and Lücke have shown that $\{1\,1\,1\}\langle 1\,1\,2\rangle$ nuclei growth preferentially into $\{1\,1\,0\}\langle 1\,1\,2\rangle$ deformed matrix because of their 27° $\langle 1\,1\,0\rangle$ coincidence relationship [10]. The component CH is absent in FSS-R grade after recrystallization annealing.

4. Summary and conclusions

The texture evolution in four ferritic stainless steels containing different amounts of niobium and interstitials was investigated. The recrystallization behavior varies significantly among grades FSS-A, FSS-B and FSS-C. Grain size also varies markedly from one region to another as well as the extent of recrystallization. Important orientation and composition effects (Nb in solid solution and interstitials) were observed and exert marked influence on the final recrystallization texture of coarse-grained ferritic stainless steels.

For the reference steel a typical $\{1\,1\,1\}\langle 1\,1\,2\rangle$ texture was found after final recrystallization annealing. In contrast, the final recrystallization texture found in coarse-grained FSS-A, FSS-B and FSS-C was significantly influenced by the microstructure developed after hot-band annealing at 1250 °C for 2 h. New texture components belonging to $\{0\,u\,v\}\langle 1\,0\,0\rangle$ and $\{0\,0\,1\}\langle u\,v\,0\rangle$ are present in these grades. We believe these changes can be explained by the initial coarse-grained structure of steel grades A to C compared to the reference steel (grade R).

Acknowledgments

The authors are indebted to FAPESP and to CNPq (Brazil) for the financial support (Grant 05/60131-5) and to Mrs. Katja Angenendt (MPI-E) for her kind assistance in the EBSD measurements.

References

[1] Steel Heat Treatment: Metallurgy and Technologies, CRC Press, Boca Raton, FL, 2007, pp. 695–735.
[2] ASM Metals Reference Book, ASM, Materials Park, OH, 1993, pp. 112–116.
[3] Steel Products Manual, Iron and Steel Society, Warrendale, PA, 1999, pp. 251–256.
[4] I. Tikhovskiy, D. Raabe, F. Roters, Mater. Sci. Eng. A488 (2008) 482–490.
[5] G.M. Sim, J.C. Ahm, S.C. Hong, K.J. Lee, K.S. Lee, Mater. Sci. Eng. A396 (2005) 159.
[6] N. Fujita, M. Kikuchi, K. Ohmura, ISIJ Int. 43 (2003) 1999–2006.
[7] C.W. Sinclair, C.R. Hutchinson, Y. Bréchet, Metall. Trans. 38A (2007) 821–830.
[8] C.R. Hutchinson, H.S. Zurob, C.W. Sinclair, Y.J.M. Brechet, Scripta Mater. 59 (2008) 635–637.
[9] M. Hölscher, D. Raabe, K. Lücke, Steel Res. 62 (1991) 567–575.
[10] D. Raabe, K. Lücke, Scripta Metall. Mater. 27 (1992) 1533–1538.
[11] N.J. Wittridge, R.D. Knutsen, Mater. Sci. Eng. A269 (1999) 205–216.
[12] D. Raabe, J. Mater. Sci. 31 (1996) 3839–3845.
[13] D. Raabe, Steel Res. 74 (2003) 327–337.
[14] B. Hutchinson, Phil. Trans. R. Soc. Lond. A 357 (1999) 1471–1485.
[15] F.J. Humphreys, M. Hatherly, Recrystallization and Related Annealing Phenomena, Pergamon Press, Oxford, 1995.
[16] T. Senuma, K. Kawasaki, ISIJ Int. 34 (1994) 51–60.
[17] P. Van Houtte, L. Delannay, S.R. Kalidindi, Int. J. Plast. 18 (2002) 359–377.
[18] P. Van Houtte, A. Van Bael, M. Seefeldt, L. Delannay, Mater. Sci. Forum 495–497 (2005) 31–41.
[19] P. Van Houtte, Mater. Sci. Eng. 55 (1982) 69–77.
[20] P. Van Houtte, S. Li, M. Seefeldt, L. Delannay, Int. J. Plast. 21 (2005) 589–624.
[21] M.Y. Huh, O. Engler, Mater. Sci. Eng. A308 (2001) 74–87.
[22] J. Hamada, Y. Matsumoto, F. Fudanoki, S. Maeda, ISIJ Int. 43 (2003) 1989–1998.
[23] M.-Y. Huh, J.-H. Lee, S.H. Park, O. Engler, D. Raabe, Steel Res. 76 (2005) 797–806.
[24] D. Raabe, M. Sachtleber, H. Weiland, G. Scheele, Z. Zhao, Acta Mater. 51 (2003) 1539–1560.
[25] N. Chen, S. Zaefferer, L. Lahn, K. Günther, D. Raabe, Acta Mater. 51 (2003) 1755–1765.
[26] S.K. Chang, Mater. Sci. Eng. A452 (2007) 93–98.
[27] P.V. Houtte, The MTM-FHM Software System V.2, User Manual, 1995.
[28] R.P. Siqueira, H.R.Z. Sandim, T.R. Oliveira, Mater. Sci. Eng. A497 (2008) 216–223.
[29] G.M. Sim, J.C. Ahn, S.C. Hong, K.J. Lee, K.S. Lee, Mater. Sci. Eng. A396 (2005) 159–165.
[30] D. Raabe, K. Lücke, Mater. Sci. Technol. 9 (1993) 302–312.
[31] M. Hölscher, D. Raabe, K. Lücke, Acta Metall. 42 (1994) 879–886.
[32] D. Raabe, Z. Zhao, S.-J. Park, F. Roters, Acta Mater. 50 (2002) 421–440.
[33] N. Tsuji, K. Tsuzaki, T. Maki, ISIJ Int. 32 (1992) 1319–1328.
[34] N. Tsuji, K. Tsuzaki, T. Maki, ISIJ Int. 33 (1993) 783–792.
[35] H.R.Z. Sandim, J.P. Martins, A.F. Padilha, Scripta Mater. 45 (2001) 733–738.
[36] H.R.Z. Sandim, D. Raabe, Scripta Mater. 53 (2005) 207–212.
[37] C.S. Lee, B.J. Duggan, R.E. Smallman, Acta Metall. Mater. 41 (1993) 2265.
[38] D.A. Hughes, in: E.N.C. Dalder, T. Grobstein, C.S. Olsen (Eds.), Evolution of Refractory Metals and Alloys, TMS, Pittsburg, 1993, p. 219.
[39] D. Raabe, Steel Res. 66 (1995) 222–229.
[40] H. Homma, B. Hutchinson, Acta Mater. 51 (2003) 3795–3805.